Challenge Journal of Concrete Research Letters

Research Article

Mechanical properties and freeze-thaw resistances of bronze-concrete composites

Tuba Bahtli [a,*], Nesibe Sevde Ozbay [b]

[a] *Department of Metallurgy and Materials Engineering, Necmettin Erbakan University, 42090 Konya, Turkey*
[b] *Department of Mechanical Engineering, Necmettin Erbakan University, 42090 Konya, Turkey*

ABSTRACT

Studies in the literature show that the physical and mechanical properties of concrete could be improved by the incorporation of different kinds of industrial waste, including waste tire rubber and tire steel. Recycling of waste is important for economic gain and to curb environmental problems. In this study, finely ground CuAl10Ni bronze is used to improve the physical and mechanical properties, and freeze-thaw resistances of C30 concrete. The density, cold crushing strength, 3-point bending strength, elastic modulus, toughness, and freeze-thaw resistances of concrete are determined. In addition, the Schmidt Rebound Hammer (SRH) and the ultrasonic pulse velocity (UPV) tests, which are non-destructive test methods, are applied. SEM/EDX analyses are also carried out. It is noted that a more compacted structure of concrete is achieved with the addition of bronze sawdust. Then higher density and strength values are obtained for concretes that are produced by bronze addition. In addition, concretes including bronze sawdust generally show higher toughness due to high plastic energy capacities than pure concrete.

ARTICLE INFO

Article history:
Received 17 December 2020
Revised 17 February 2021
Accepted 17 March 2021

Keywords:
Bronze sawdust
Composite
Concrete
Damage analysis
Freeze-thaw
Mechanical behavior

1. Introduction

Concrete is the most commonly used construction material, which is produced by a proportioned mixture of cement, sand and gravel or other fine or coarse aggregates and water, then hardened in forms in the shape of desired structures (Nilson and Winter, 1991).

Concrete does not always satisfy requirements, including low density, high toughness, and high impact resistance (Topçu, 1995). Reinforcement, especially round steel rods, is placed in forms in advance of the concrete to provide interlocking (Nilson and Winter, 1991). The addition of steel fibers as reinforcement in concrete, provides improvement in most mechanical properties (Ramakrishnan and Coyle, 1983; Balaguru and Ramakrishnan, 1987; Ramakrishnan and Coyle, 1983).

Waste materials have recently been employed in concrete structures in order to improve the physical properties of the concrete (Topçu, 1995). It is important to investigate other sources of raw materials in order to achieve a greener concrete by reducing the consumption of natural resources (Rahal, 2007). The authors believe that recycled steel bead concrete will have better mechanical properties than that of concrete made with the addition of recycled tire products (Bignozzi and Sandrolini, 2006). Similarly, results from a number of studies suggest that a loss in strength could be minimized through the use of rubber tire particles, which can lead to environmental problems (Lee et al., 1993; Raghavan et al., 1998; Li et al., 1998; Segre and Joekes, 2000). However, rubberized concrete generally shows greater toughness than traditional concrete (Bignozzi and Sandrolini, 2006).

The service life of concrete structures, and also the deterioration of concrete when subjected to multi-damaging processes, such as freeze-thaw cycling and chloride attacks, are also quite important (Sun et al., 2002). Water that penetrates into the porosities of concrete is the main cause of degradation of building materials. When concrete is subjected to temperature cycles, as temperature lowers, water freezes to ice and expansion of voids

* *Corresponding author*. Tel.: +90-332-325-2024 ; E-mail address: taksoy@erbakan.edu.tr (T. Bahtli)
ISSN: 2548-0928 / DOI: https://doi.org/10.20528/cjcrl.2021.02.001

occur, whereas when the temperature increases ice melts to water, so the concrete deteriorates rapidly due to freezing and thawing (Polat et al., 2010).

In this study, with the addition of bronze that could adapt to a concrete structure with its Al content, improving mechanical properties, certain thermal properties such as the freeze-thaw resistance of concrete is researched. There has been no study to date in the literature on the use of bronze waste in concrete.

Damage analysis in composite materials after experimental study is extremely important in material in order to identify composite components and predict damage behavior in similar studies that will be designed (Gemi et al., 2019; Gemi et al., 2017; Özkılıç et al., 2020). The interface formed between the reinforcement and matrix components in composite materials, homogeneous structures and toughness mechanisms could be determined by micro damage analysis. In the literature, there have been many studies on the damage analysis of composite materials during and after experimentation. In general, micro cracks, pull-out, debonding, reinforcement and matrix damage have been observed (Gemi et al., 2018; Madenci et al., 2020; Gemi et al., 2020). In these studies, damage modes were determined by examination of general damage occurring between the composite and the composite components.

2. Materials and Method

C30 class dry ready mixed concrete was used in the experimental work. Finely ground CuAl10Ni bronze (Fig. 1-a and -b), that was prepared by grinding in a ring mill for three minutes, was used as an additive material. After the C20 dry mixed concrete and ground CuAl10Ni bronze additives were weighed, they were mixed in a concrete mixer (Fig. 1-c) in a dry form for one minute without the addition of water. After this mixing, water was added up to 10% of the cement ratio and it was then mixed for five more minutes. After ensuring a homogeneous mixture, the concrete mortar was shaped by manual compression into metal molds (Fig 1-d and -e).

Concrete cubes of 5 cm^3 in size, that were either pure or which incorporated 1%, 3% and 5% by mass of bronze sawdust were prepared for physical, cold crushing and freeze-thaw tests. In addition, 25mm × 25mm × 150mm beam samples were prepared for a three-point bending test.

(a) (b) (c) (d) (e)

Fig. 1. a) CuAl10Ni sawdust; b) Finely ground CuAl10Ni sawdust; c) Concrete mixer; d) and e) Metal molds.

All of the shaped concrete samples were cured for twenty-eight days in water. Open porosity and density measurements using the Archimedes principle (ASTM C-642), cold crushing tests (ASTM C-109) for 5 cm^3 concrete blocks, and a 3-point bending test (ASTM C-78) for 25 mm×25 mm×150 mm beam concrete samples by the Shimadzu AGS-X device were performed, as can be seen in Fig. 2.

Fig. 2. 3-point bending test: a) Test machine; b) Test sample.

For the Schmidt Rebound Hammer (SRH) test method, the average compressive strength values of the samples were determined. In addition, the speed of the sound waves was determined by the ultrasonic pulse velocity (UPV) test as a function of the porosities.

Freeze-thaw resistance tests for 5 cm^3 concrete blocks were conducted according to the ASTM C-666 standard, using a freeze-thaw test cabinet at temperatures of between -20°C and +20°C, totaling a 150-minute freeze-thaw cycle. Ten, twenty-five and fifty freeze-thaw cycles were applied, respectively. At the end of the experiment, the mass loss and the cold crushing strength (CCS) results were examined. After the freeze-thaw test, the strength ratio (the percentage of retained strength) values for each material were calculated.

3. Results and Discussion

3.1. Physical and mechanical properties of the concrete

The physical and mechanical properties of the C30 class concrete samples, obtained for cubes measuring 5 cm^3 in dimension and cured for twenty-eight days in water, are given in Tables 1 and 2.

Table 1. Density, open porosity and mechanical properties (cold crushing strength) of concrete samples produced with the bronze sawdust additive (C: Concrete, B: Bronze).

Material	Density (g/cm^3)	Open Porosity (%)	Cold Crushing Strength (MPa)
C	2.35	8.82	63.64
C+1%B	2.37	8.78	65.48
C+3%B	2.41	8.71	66.20
C+5%B	2.42	8.38	67.76

Table 2. Results of strength according to the Schmidt Rebound Hammer test (SRH) and the speed of the sound waves obtained from the ultrasonic pulse velocity (UPV) tests.

Material	Average strength (MPa)	The speed of sound (m/s)
C	53.57	4567
C+5%B	57.24	4571

According to the results, the average density, open porosity, and CCS values of unreinforced concrete are 2.35 g/cm^3, 8.82%, and 63.64 MPa, respectively. Generally, the density and CCS values of the unreinforced concrete increased with the bronze sawdust additives, while the amount of open porosity decreased. Strength values were increased due to density values which also increased. According to Nagrockiene et al. (2017), zeolite (hydrous alumino silicates) has a positive effect on compressive strength, and density. It is thought that strong interfacial bonds could be achieved between the concrete and bronze sawdust due to the compatibility of aluminum content of each material. Maximum density and mechanical properties were achieved in the C+5%B material.

According to Siddique et al. (2007), with the inclusion of finer used foundry sand (UFS) rather than regular sand results in a denser concrete matrix, and also an increase in compressive strength. Similarly, in our study, finely ground bronze sawdust could also fill the pores, causing an increase in density and strength.

Generally, more compact concrete structure was obtained by increasing the amount of bronze added, as can be seen in Fig. 3. Furthermore, deep cracks were seen in pure concrete (Fig. 3-a), and microcracks were seen in concrete that had been produced by the addition of bronze (Fig. 3-b-d). In addition, the depth of the microcracks decreased with an increase in bronze content. These microcracks also could provide higher strength due to their smaller depth and greater toughness by acting as a barrier to newly-formed cracks or microcrack bridging.

The SRH strength and the speed of the sound wave results (UPV tests) are given in Table 2. Concrete produced with the addition of 5% bronze sawdust had greater strength than unreinforced concrete, similar to CCS values. As the porosity of the samples increased, strength

increased and the speed of sound passing through these samples decreased.

According to the 3-point bending test results (Fig. 4), the strength and toughness values of the concrete increased, while the elastic modulus values decreased with the addition of bronze sawdust.

It is thought that plastic energy capacities began to increase with the addition of bronze. Greater strength and toughness are the result of concrete samples incorporating finely ground bronze sawdust due to their high plastic energy compared to pure concrete. The main brittle concrete matrix was strengthened by the addition of more ductile bronze.

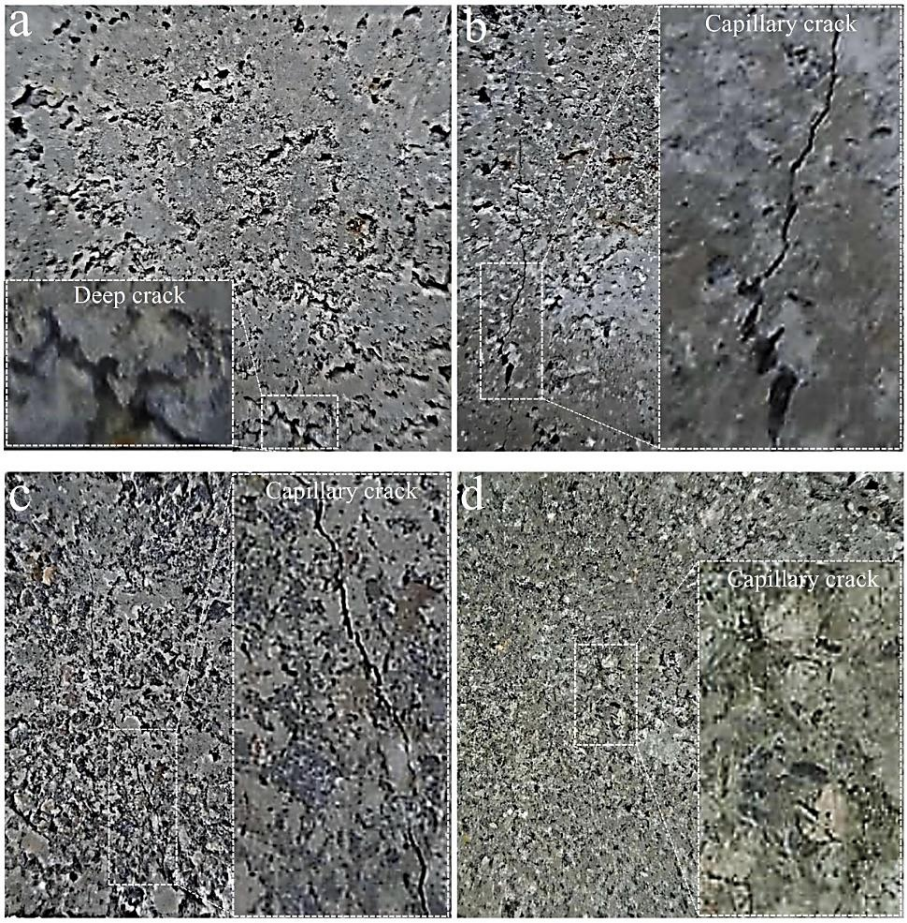

Fig. 3. 5 cm^3 square prism concrete materials: a) Pure C; b) C+1%B; c) C+3%B; d) C+5%B.

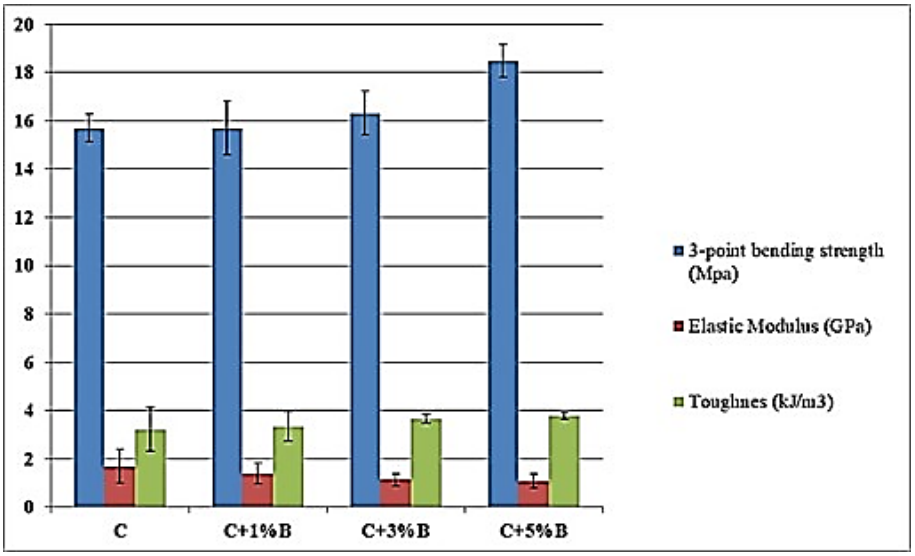

Fig. 4. 3-point bending test results of the concrete.

3.2. SEM analysis of concrete samples

Even though porosities and microcracks, generally denser in structure for unreinforced concrete, can be seen (Fig. 5-a). Strong bonding can be observed at the interfaces between the white color bronze grains and the gray concrete matrix grains in Fig. 5.

This confirms the idea that the density of this concrete, that was prepared with a 5% bronze sawdust addition, is close to that of the unreinforced concrete sample. It is thought that the CCS, 3-point bending and toughness values increased because there was no significant decrease in density and the bronze material was ductile (Fig. 6). In addition, the distribution of Cu, Al, Ni elements are in the same region, and these granules are with the addition of bronze sawdust in Fig. 7.

According to the distribution of elements in the concrete samples (Table 3), it can be seen that Ca, Si, Al, that are present in the cement phases, exist predominantly in pure concrete. While concrete containing bronze sawdust has a higher content of Cu, Al, Ni elements, these were the main constituents of the bronze material.

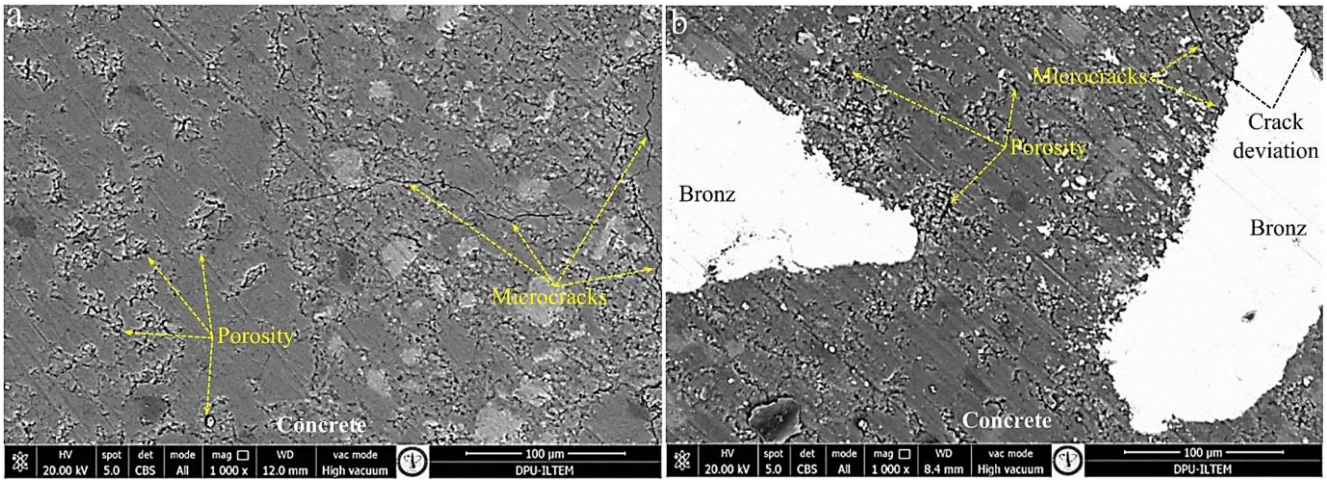

Fig. 5. SEM images of: a) Unreinforced (C); b) C+5%B (1000X)**.**

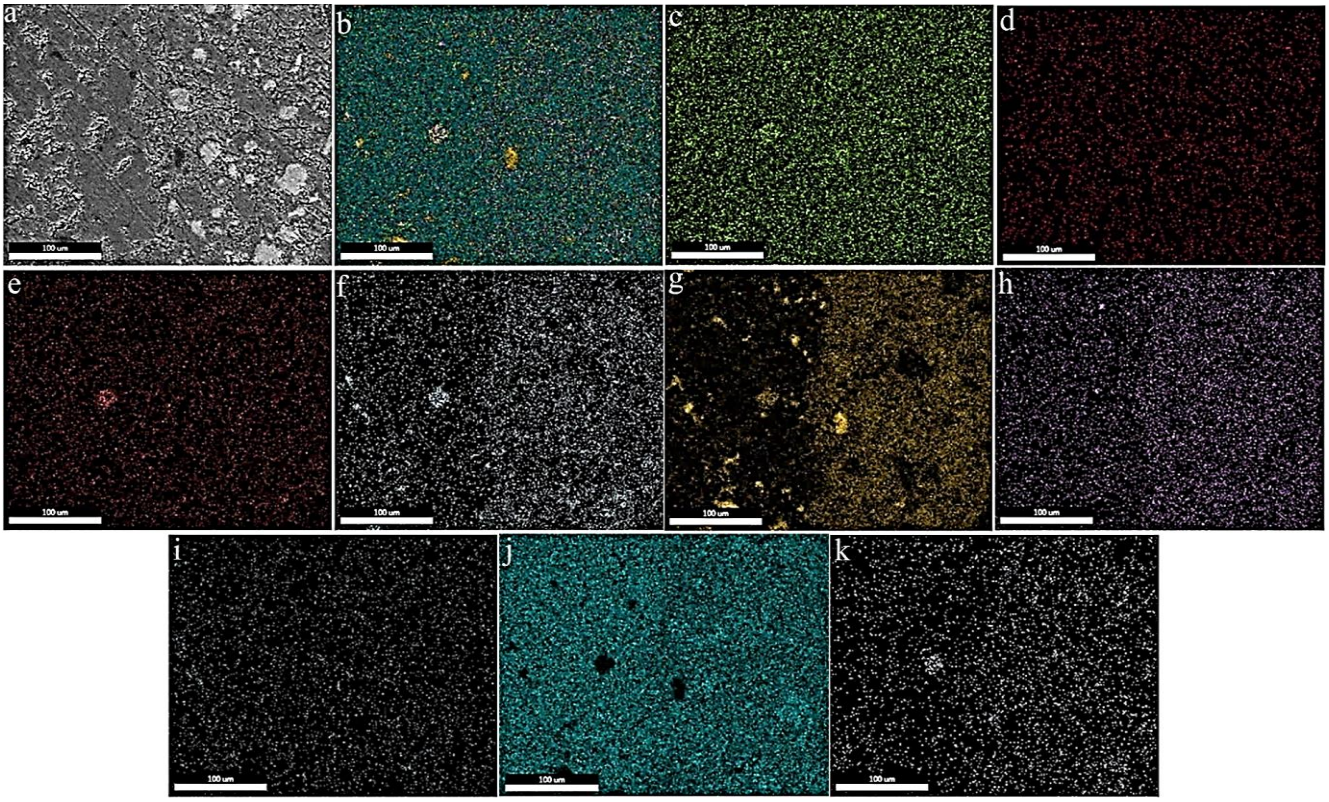

Fig. 6. a) Microstructure; b) Colored microstructure, elemental distribution of pure concrete; c) O; d) Na; e) Mg; f) Al; g) Si; h) S; i) K; j) Ca; k) Fe (1000X).

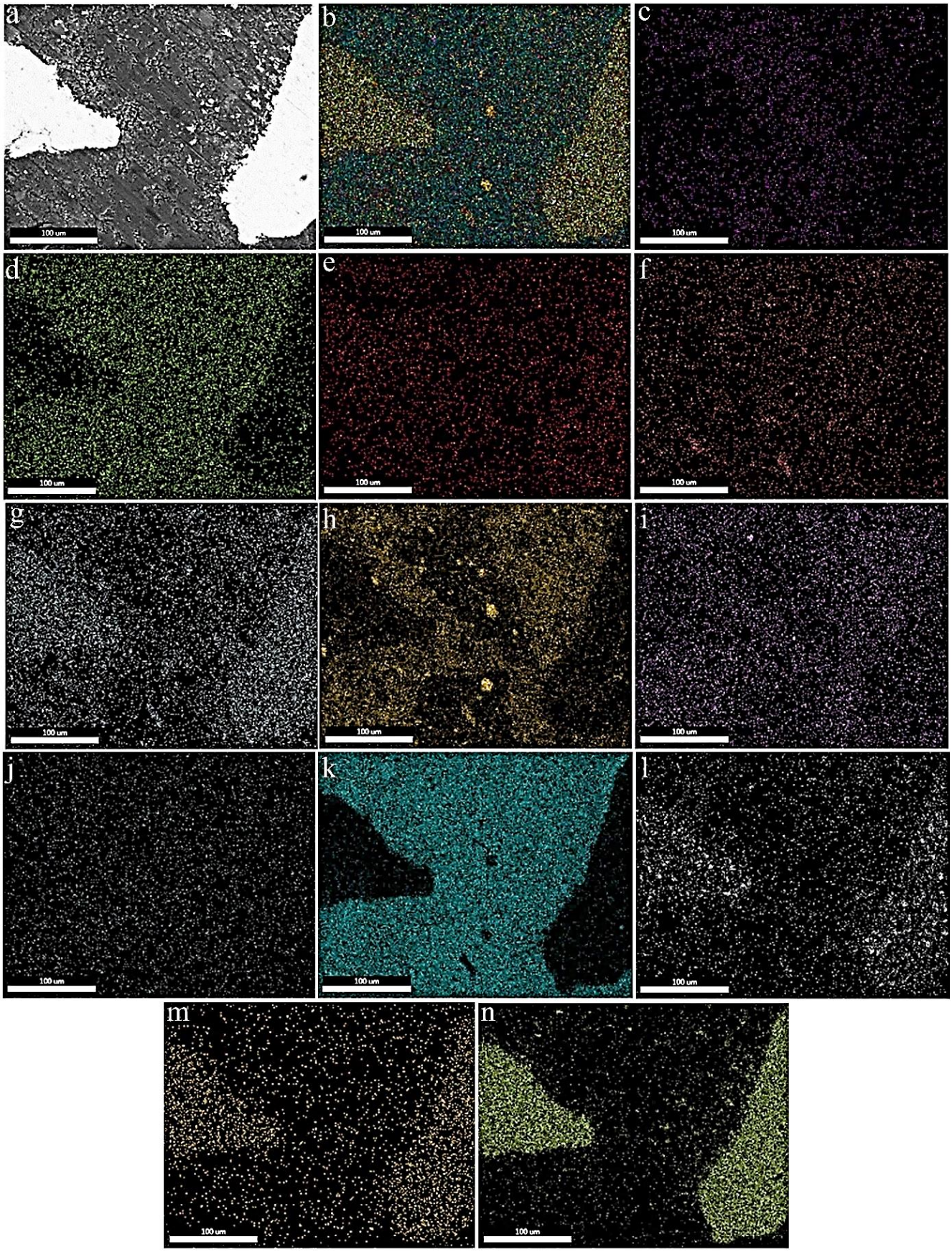

Fig. 7. a) Microstructure; b) Colored microstructure, elemental distribution of pure C+5%B; c) C; d) O; e) Na; f) Mg; g) Al; h) Si; i) S; j) K; k) Ca; l) Fe; m) Ni; n) Cu (1000X).

Table 3. EDX analysis of concrete samples.

Elements (%)	Materials	
	C	C+5%B
O	14.39	10.07
Na	1.26	1.15
Mg	2.59	1.13
Al	4.13	6.13
Si	12.04	9.74
S	3.19	4.89
K	2.1	2.49
Ca	58.97	32.87
Fe	1.43	3.47
Ni	0	2.24
Cu	0	25.82

3.3. Freeze-thaw results

The CCS and strength ratio of the concrete samples after ten, twenty-five and fifty freeze-thaw cycles are given in Fig. 8.

Generally, the CCS values decreased as the number of freeze-thaw cycles increased due to the content of structural defects, such as porosity and microcracks, increasing. Neither pure concrete nor concrete incorporating bronze sawdust, could further retain strength values with the freeze-thaw cycles. This means that the energies of new microcracks, formed after the freeze-thaw cycles, were not absorbed by the concrete.

After the freeze-thaw test, the mass of pure concrete material decreased gradually with the freeze-thaw cycles, due to an increase of structural defects. On the other hand, the weight of the bronze-added concrete material slightly increased (Table 4).

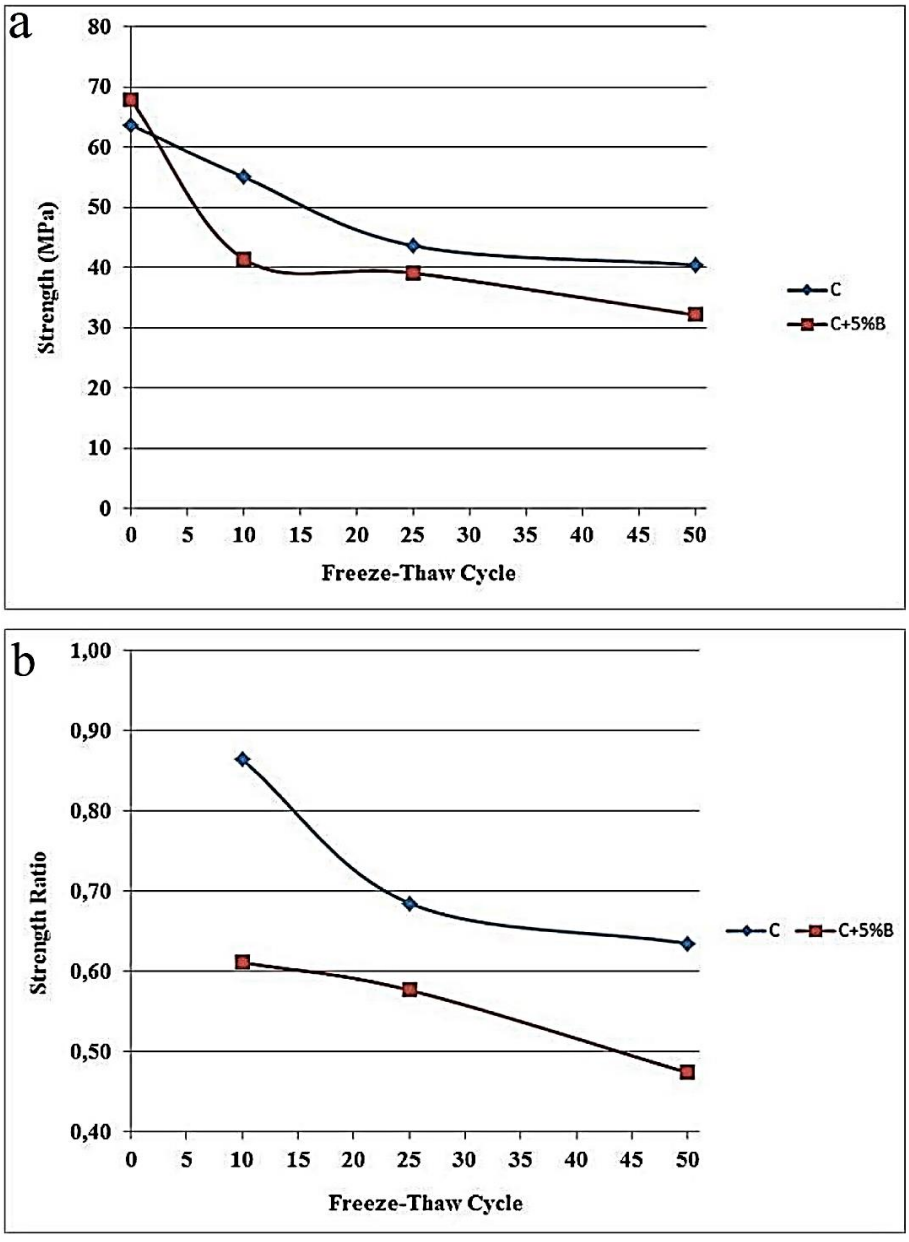

Fig. 8. a) Strength and b) strength ratio values of the concretes according to freeze-thaw cycles after freeze-thaw testing.

Table 4. Mass measurements of samples subjected to freeze-thaw cycles.

Material	Mass before freeze-thaw test (g)	Mass after 10 freeze-thaw cycle (g)	Mass after 25 freeze-thaw cycle (g)	Mass after 50 freeze-thaw cycle (g)
C	302.77	299.08	298.54	293.68
C+5%B	316.81	319.22	316.71	316.32

According to the SEM images that can be seen in Fig. 9, and an EDX analysis (Table 5) of the concrete after the freeze-thaw tests, it was found that the concrete matrix was affected by the freeze-thaw tests, with a loss of material, particularly with the percentages of Ca and Si decreasing. In the case of the bronze doped concrete, the decrease in the percentage of Ca and Si caused an increase in oxygen and Cu percentages.

When the colored microstructure and elements distribution were examined, it was seen that the content of oxygen and bronze was not high in the same regions, meaning that the bronze particles were slightly oxidized. However, the Cl ions were in the regions where both the concrete matrix and the Cu element were present. It was thought that chloride ions entered into the concrete matrix and a type of corrosion known as bronze cancer, a chemical change caused by copper and its alloys and chloride ions, had occurred. These changes are thought to cause a mass gain of concrete materials. During the bronchial cancer process, free chlorine ions react with each other to form copper (I) chloride, called nantocite, as a first layer on the metal surface.

$$2Cu^{+} + 2Cl^{-} \rightarrow Cu_2Cl_2$$

or

$$Cu^{+} + Cl^{-} \rightarrow CuCl \text{ (nantocite)}$$

In the presence of chlorine ions, nantocite converts to basic copper (II) chloride in a humid and oxygenated environment (Ozbay, 2018).

$$2Cu_2Cl_2 + 4H_2O + O_2 \rightarrow CuCl_2{\cdot}3Cu(OH)_2 + 2HCl$$

Hydrochloric acid HCl, which is released as a result of this reaction, reacts with oxygen to create metallic corrosion.

$$2CuO + 2HCl + \tfrac{1}{2}O_2 \rightarrow Cu_2Cl_2 + H_2O$$

$$Cu_2O + 2HCl \rightarrow Cu_2Cl_2 + H_2O$$

Reactions continue until all the metal corrosion and stabilized metal corrosion products are converted into basic copper (II) chloride (Ozbay, 2018).

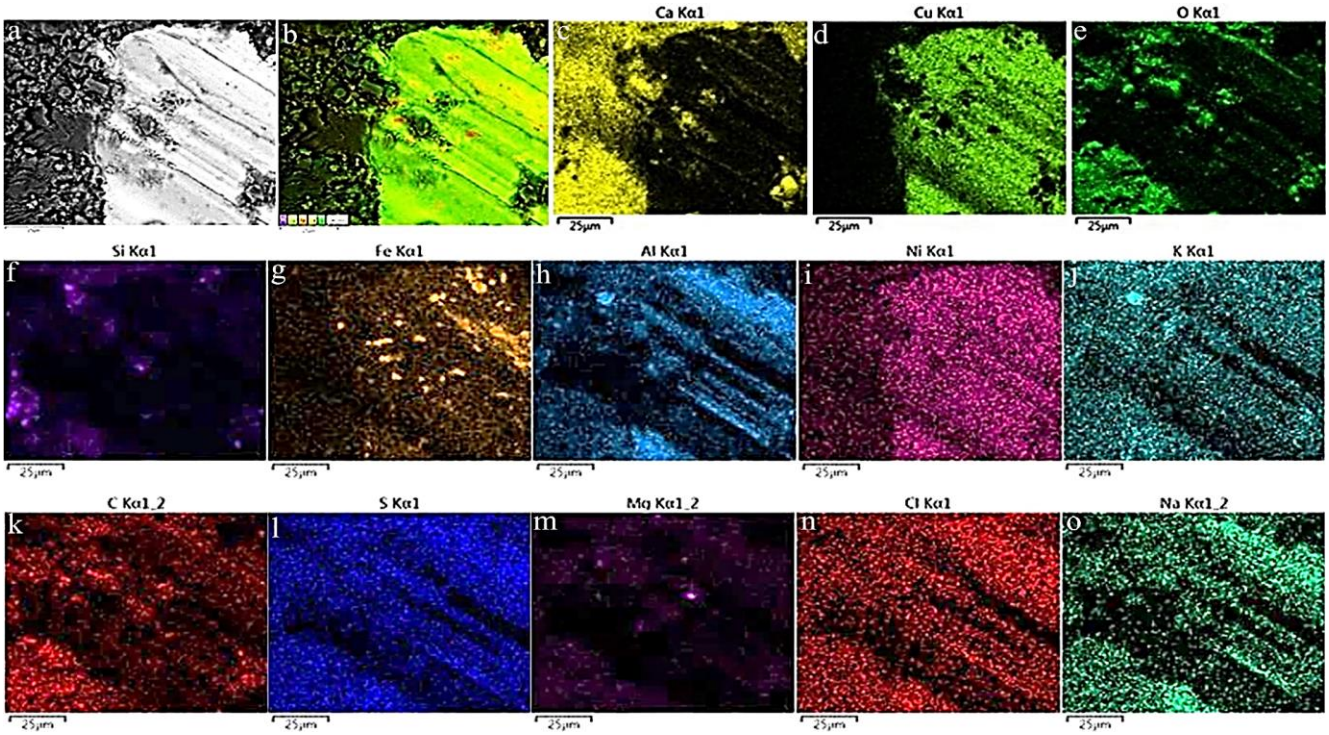

Fig. 9. After freeze-thaw test: a) Microstructure; b) Colored microstructure, elemental distributions of C+5%B; c) Ca; d) Cu; e) O; f) Si; g) Fe; h) Al; i) Ni; j) K; k) C; l) S; m) Mg; n) Cl; o) Na (1000X).

Table 5. EDX analysis of C+5%B material before and after freeze-thaw testing.

Element	Before freeze-thaw test (%)	After freeze-thaw test (%)
O	10.07	18.54
Ca	32.87	15.73
Fe	3.47	4.41
Ni	2.24	3.31
Cu	25.82	51.09
Cl	0	0.05
Na	1.15	0.28
Mg	1.13	0.78
K	2.49	0.50
Al	6.13	2.84
Si	9.74	2.48
S	4.89	0.01

Fracture surface images of the concrete materials, before and after the freeze-thaw test, are given in Fig. 10. Before the freeze-thaw test, transgranular cracks for pure concrete were dominant, but after the freeze-thaw test, generally both the transgranular and intergranular cracks were found in pure material. Transgranular and intergranular cracks, dominantly transgranular crack for bigger grains, were observed together in the C+5%B material, both before and after the freeze-thaw tests. This transition from an intergranular fracture type to a transgranular fracture type was also influenced by a decrease in mechanical properties.

4. Conclusions

The highest density, strength and toughness values were obtained for C+5%B concrete, due to the ductility of the bronze and filling of the concrete voids with the addition of bronze.

The energies of new microcracks formed after the freeze-thaw cycles were not absorbed by either pure concrete or concrete incorporating bronze sawdust. It can be concluded that the water absorption of the concrete incorporating bronze sawdust could cause a mass increase in the microstructure change as a result of a freeze-thaw action application. According to SEM-mapping images of C+5%B, the Cl ions were in the regions where both the concrete matrix and the Cu element were present. This indicates that chloride ions entered into the concrete matrix and corrosion, known as bronze cancer, occurred.

Acknowledgements

This study was supported by Necmettin Erbakan University Scientific Research Projects under Project No. 171351001.

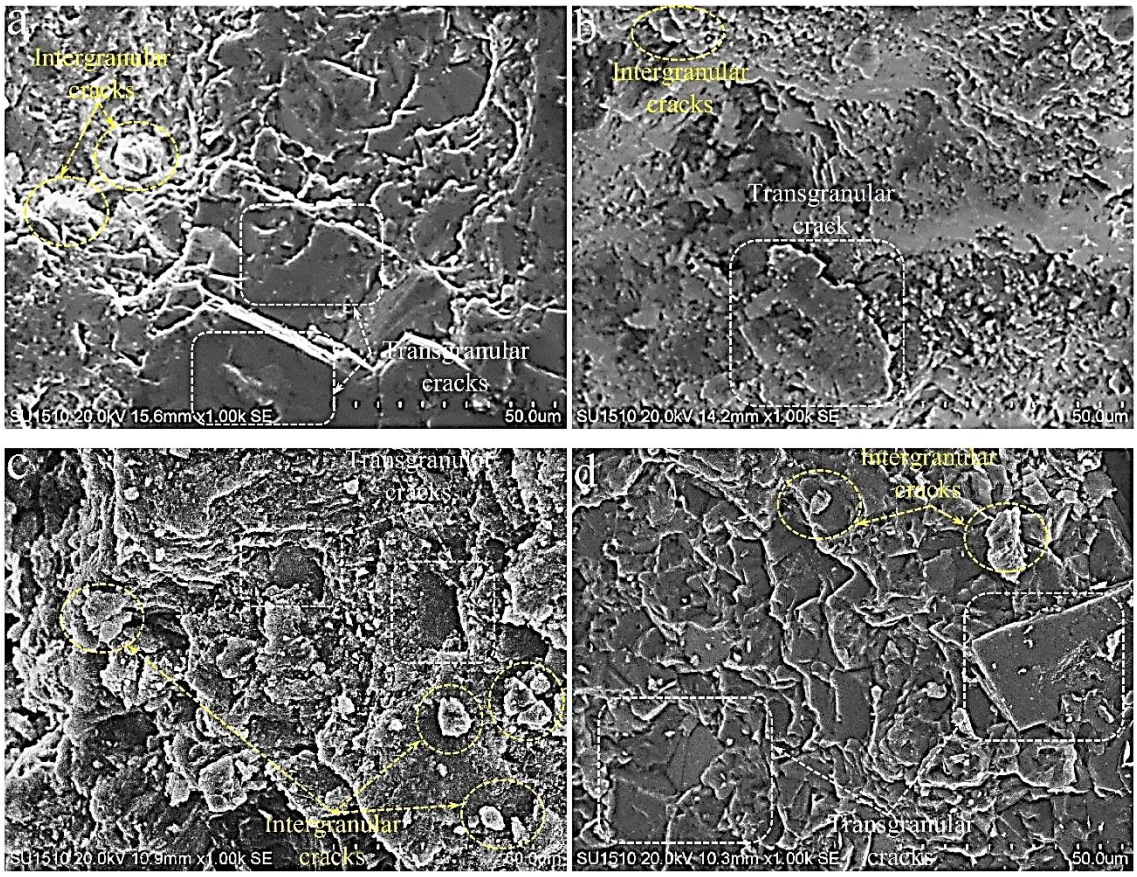

Fig. 10. Fracture surface images before freeze-thaw test:
a) C; b) C+5%B and fracture surface analysis after freeze-thaw test; c) C; d) C+5%B (1000X).

REFERENCES

Balaguru P, Ramakrishnan V (1987). Comparison of slump cone and V-B tests as measures of workability for fiber reinforced and plain concrete. *Cement Concrete Aggregates*, 9(1), 3-11.

Bignozzi MC, Sandrolini F (2006). Tyre rubber waste recycling in self-compacting concrete. *Cement and Concrete Research*, 36(4), 735-739.

Gemi L, Yazman S, Uludağ M, Dispinar D, Tiryakioğlu M (2017). The effect of 0.5 wt% additions of carbon nanotubes & ceramic nanoparticles on tensile properties of epoxy-matrix composites: a comparative study. *Materials Science and Nanotechnology*, 1(2), 15-22.

Gemi L, Köroğlu MA, Ashour A (2018). Experimental study on compressive behavior and failure analysis of composite concrete confined by glass/epoxy ±55° filament wound pipes. *Composite Structures*, 87, 157-68.

Gemi L, Aksoylu C, Yazman Ş, Özkılıç YO, Arslan MH (2019). Experimental investigation of shear capacity and damage analysis of thinned end prefabricated concrete purlins strengthened by CFRP composite. *Composite Structures*, 229, 111399.

Gemi L, Morkavuk S, Köklü U, Yazman Ş (2020). The effects of stacking sequence on drilling machinability of filament wound hybrid composite pipes: Part-2 damage analysis and surface quality. *Composite Structures*, 235, 111737.

Lee BI, Burnett L, Miller T, Postage B, Cuneo J (1993). Tyre rubber/cement matrix composites. *Journal of Materials Science Letters,* 12(13), 967-968.

Li Z, Li F, Li JSL (1998). Properties of concrete incorporating rubber tyre particles. *Magazine of Concrete Research*, 50(4), 297-304.

Madenci E, Özkılıç YO, Gemi L (2020). Experimental and theoretical investigation on flexure performance of pultruded GFRP composite beams with damage analyses. *Composite Structures*, 242, 112162.

Nagrockiene D, Girskas G, Skripkiunas G (2017). Properties of concrete modified with mineral additives. *Construction and Building Materials,* 135, 37-42.

Nilson AH, Winter G (1991). Design of concrete structures. MCGraw-Hill, Inc., 11th Edition, Singapore.

Ozbay NS (2018). İnce Öğütülmüş Bronz, Tel ve Lastik Atıkları ile Üretilen Betonun Soğuk Basma Mukavemeti, Korozyon ve Donma-Çözülme Direncinin Araştırılması. Graduate Thesis, Necmettin Erbakan University, Konya, Turkey. (in Turkish)

Özkılıç YO, Madenci E, Gemi L (2020). Tensile and compressive behaviors of the pultruded GFRP Lamina. *Turkish Journal of Engineering* (*TUJE*), 4, 169-175.

Polat R, Demirboğa R, Karakoç MB, Türkmen I (2010). The influence of lightweight aggregate on the physico-mechanical properties ofconcrete exposed to freeze–thaw cycles. *Cold Regions Science and Technology*, 60(1), 51-56.

Raghavan D, Huynh H, Ferraris CF (1998). Workability, mechanical properties and chemical stability of a recycled tyre rubber-filled cementitious composite. *Journal of Materials Science,* 33, 1745-1752.

Rahal K (2007). Mechanical properties of concrete with recycled coarse aggregate. *Building and Environment*, 42, 407-415.

Ramakrishnan V, Coyle WV (1983). Steel fiber reinforced super-plasticized concretes for rehabilitation of bridge decks and highway pavements. Final Report to U.S. Department of Transportation, DOT/RSPA/DMA-50, 84(2), p. 408.

Segre N, Joekes I (2000). Use of tire rubber particles as addition to cement paste. *Cement and Concrete Research*, 30(9), 1421-1425.

Siddique R, Schutter G, Noumowe A (2007). Effect of used-foundry sand on the mechanical properties of concrete. *Construction and Building Materials,* 23(2), 976-980.

Sun W, Mu R, Luo X, Changwen M (2002). Effect of chloride salt, freeze–thaw cycling and externally applied load on the performance of the concrete. *Cement and Concrete Research*, 32(12), 1859-1864.

Topçu İB (1995). The properties of rubberized concretes. *Cement and Concrete Research*, 25(2), 304-331.